Oxidation kinetics of Ti6Al4V alloy deposited by wire arc additive manufacturing using Ar gas as processing atmosphere

J. E. Ordaz-Cervantes, R. Morales-Estrella* and N. Ortiz-Lara

Instituto de Investigaciones Metalúrgicas,
Edificio U, Universidad Michoacana de San Nicolás de Hidalgo,
**e-mail: ricardo.morales@umich.mx*

E. Reyes-Gordillo

Departamento Metal-Mecánica,Tecnológico Nacional de México, Insituto Tecnológico de Morelia,
Formerly, a PhD student with Instituto de Investigaciones Metalúrgicas, Edificio U,
Universidad Michoacana de San Nicolás de Hidalgo, Gral. Francisco J. Múgica
Consejo Nacional de Ciencia y Técnología,
Av. Insurgentes 1582, Crédito constructor, Ciudad de México 03940

D. G. Espinosa-Arbeláez

Centro de Ingeniería y Desarrollo Industrial (CIDESI), Querétaro, 76125, México.

Received 1 December 2022; accepted 4 March 2024

Ti6Al4V alloy is currently the most common metal alloy of the $\alpha + \beta$ phase type, its application is increasing as it has excellent properties at elevated temperatures. The main users of Ti6Al4V alloy are industries such as aerospace, naval, and biomedical; therefore, Ti6Al4V alloy is one of the most studied material worldwide to manufacture low weight and corrosion resistant components. One of the great advantages that Ti6Al4V alloy offers is the possibility of manufacturing components in situ by means of additive technologies. Similar studies, in additive manufacturing, have reported the formation of titanium oxide on the surface of the material, followed by an oxygen-enriched region called "α-case". By means of thermogravimetric analysis, the oxidation effect on the surface of Ti6Al4V samples, obtained by wire arc additive manufacturing as well as samples from conventional manufacture, were studied. Argon gas, with an oxygen partial pressure of 1×10^{-5} atm, was used as the oxidation atmosphere within a range of 823 to 1223K (550°C to 950°C) and oxidation times of 60 min and 180 min. For the oxidation reaction, the kinetic analyses led to calculate the activation energy as 250 kJ/mol and 166 kJ/mol for the Ti6Al4V alloy processed by conventional and additive manufacturing, respectively. The results of the thermogravimetric analyses were fitted to a parabolic-type kinetic model. Furthermore, a mathematical model was proposed to predict the oxidation kinetics. The experimental data were fitted to the mathematical model in the range of 1023-1223K (750-950°C) for Ti6Al4V alloy by wire arc additive manufacturing. The oxidized micro-structures were analyzed by optical and scanning electron microscopy (SEM) finding α-case on the surface of the samples.

Keywords: Ti6Al4V Alloy; oxidation kinetics; thermogravimetric analysis; WAAM; additive manufacturing; argon atmosphere.

DOI: https://doi.org/10.31349/RevMexFis.70.051602

1. Introduction

Wire arc additive manufacturing (WAAM) is a directed energy deposition (DED) technique that uses the continuous feeding of metal wire and an electric arc as a heat source [1]. The wire end is molten and deposited layer by layer to form an additively manufactured product [2]. WAAM technologies provide economic benefits over other additive manufacturing (AM) methods that require gas protection systems such as those required for powder feeding [3]. WAAM processes incorporate variants for each conventional electric arc welding system, such as Plasma Arc Welding (PAW) [4], Gas Tungsten Arc Welding (GTAW) [5], and Gas Metal Arc Welding (GMAW) [6]. The reduction of the thermal load in the WAAM process proposed by the Cold Metal Transfer (CMT) modification from the conventional process GMAW was included by Fronius [7] to reduce the amount of splashes, which increases the transfer efficiency, as well as the deformation of the deposit [8]. Therefore, the WAAM-CMT mixed technique exhibits the highest deposition efficiency for all additive manufacturing (AM) techniques [9].

The manufacturing of elements by WAAM has been used for the development of components, for the aerospace, aeronautics, and biomedical industry, based on titanium and aluminum alloys due to their excellent mechanical properties and density [10]. Current research on WAAM has mainly been focus on process design, micro-structure evolution and mechanical properties of the Ti6Al4V [11]. Suraj Paicker *et al.* [12] and Thapliyal *et al.* [13] reported low functional reliability of the products obtained by WAAM due to the lack of understanding about the effects of the process parameters on the micro-structure and mechanical properties produced by thermal phenomena during material deposition. Therefore, research on CMT-WAAM technique should be focused on the improvement of mechanical properties at high temperatures by understanding the degree of surface modification

promoted by oxidation.

Due to the high affinity of oxigen for titanium Caballero *et al*. [14] reported that oxidation is often observed during the WAAM process, as well as for conventional manufacturing as reported by Guleryus *et al*. [15]. Both investigations found that the depth of the oxygen diffusion zone (ODZ) increases with temperature and processing time. Also, oxygen is a stabilizing element of the α phase that leads to a larger region of diffusion within the surface zone of the material [16]; therefore, there would be a strong adsorption and greater penetration of oxygen into the matrix of Ti alloy [17], forming a fragile interstitial solid solution called α-case which downgrades the mechanical properties [16,17]. In general, few oxidation publications are reported for AM processes, the group of Antonie Casadebaigt, studied the oxidation of the alloy Ti6Al4V manufactured by Electron Beam Melting (EBM) [18] and Laser Beam Melting (LBM) [19]; they obtained activation energies for the oxidation reaction of 250 kJ/mol and 219 kJ/mol, respectively. Furthermore, they found that the oxidation kinetics obeyed the parabolic behavior of Wagner's model and further described by Khanna *et al*. [20]. From the Wagner model and linear regression analysis, it is possible to describe the change in the oxidation rate by using a mathematical expression as suggested by Dong *et al*. [17].

In the present work, the oxidation kinetics of the deposits of Ti6Al4V by WAAM-CMT and plate produced by conventional manufacture were studied using Ar atmosphere with an oxygen partial pressure of 1×10^{-5}atm. For both kind of samples, the activation energy was determined by thermogravimetric analyses using a high-precision thermobalance. In addition, metallographic analyses were performed before and after the oxidation process.

2. Methodology

2.1. Samples manufacturing

The specimens for this study were obtained from a plate of commercial condition while thin walls were additively fabricated by means of CMT-WAAM using ErTi5 (titanium Grade 5 also known as Ti6Al4V) wire. Both conditions had a chemical composition concurrent with ASTM F22924-14 [21] standard corresponding to Ti6Al4V (see Table I). The manufacturing method for thin walls was a cold metal transfer cell constituted by a VR 7000 CMT transformer manufactured by Fronius. The CMT cycle parameters were controlled by means of a RCU5000 unit. A welding torch attached to a 6-axis robotic arm (FANUC-Mate120iC) was used to melt the wire feed stock to build 3D walls. The robotic arm is located at the National Consortium for Additive Manufacturing (CONMAD) in Mexico. The deposit manufacturing parameters are described in Table II. A coaxial flow of Ar gas (99.998%) was supplied through the welding torch.

TABLE I. Chemical composition of Ti6Al4V (%wt). (1) Chemical composition ASTM F22924-14 [21], (2) Chemical composition of plate, (3) Chemical composition of CMT-WAAM deposit.

	Al	V	Fe	C	O	N	H	Ti
(1)	5.5-6.5	3.5-4.5	0.25	0.08	0.13	0.05	0.012	Bal
(2)	5.5	3.5	0.22	0.05	0.12	0.03	0.015	Bal
(3)	5.6	3.5	0.20	-	0.10	0.03	0.012	Bal

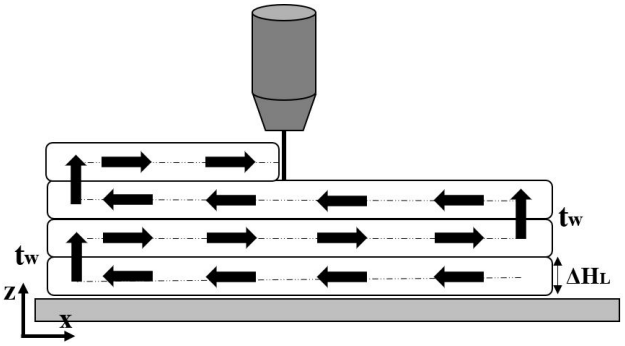

FIGURE 1. Schematic diagram of the deposit strategy for the manufacture of multilayer walls with alternating trajectory, variable interlayer time (tw), and height increment in layer-by-layer (ΔH_L) construction.

TABLE II. Parameters set for CMT-WAAM deposit.

Layers	Heat input	Interpass time	Avg. current	Feeder rate	Ts
12	207 (J/mm)	30 (seg)	115 (A)	55 (m/min)	10 (mm/s)

Figure 1 shows the deposition strategy following a zigzag path with 30 seconds of interpass time (tw) and upset (HL) increment of 5.5 mm to assure al least 20% of metallurgical dilution between the previous and the subsequent layer. The samples were cut in smaller sections with dimensions of $5 \times 10 \times 7$ mm employing a Buehler-Isomet equipment with Struers MOD 13 diamond blade. After cutting, the samples were weighed on a Mettler Toledo AB135-S/Fact precision analytical balance to record the initial weight.

2.2. Thermogravimetric Analysis (TGA)

The weight gain was obtained using a Setaram Setsys Evolution 16/18 thermogravimetric balance with an accuracy of ± 0.03 μg. The oxidation times were 60 and 180 min within a temperature range from 823 to 1223 K (550 - 950°C) with intervals of 100 K. The oxidation processing cycles are depicted in Fig. 2, which were performed under an inert atmosphere of Ar gas with an oxygen concentration 1×10^{-5} atm and a constant flow of 0.3 mL/min which was fed from the bottom of the reactor. The furnace reactor was made of alumina with an inner diameter of 18 mm wherein the sample was suspended by a 0.4 mm platinum wire basket. Temperature of the reaction chamber was monitored by means of an

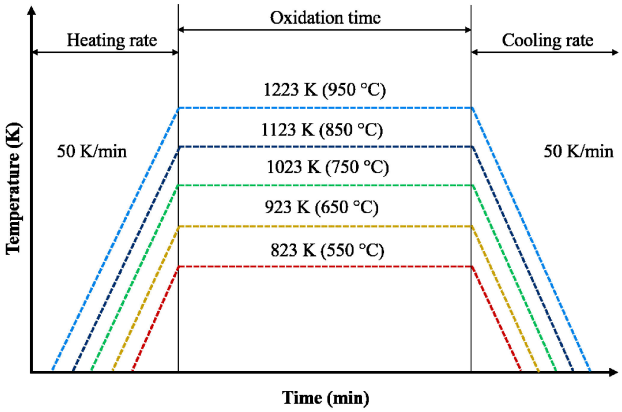

FIGURE 2. Overall thermal cycles for the oxidation of Ti6Al4V samples at several isothermal temperatures. Each isothermal section was performed at 60 and 180 min.

S-type thermocouple located just below the suspended sample.

2.3. Characterization

Samples of Ti6Al4V were subjected to metallographic analyses according to ASTM E3-01 standard with abrasive SiC and etched with chemical reagent Kroll's (H_2O 92%, HNO_3 6%, and *HF* 2%). The prepared samples were subjected to X-ray diffraction analysis (XRD) using a Rigaku SmartLab diffractometer equipped with Bragg-Brentano geometry operated at 50 kv and 30 mA through CuKα radiation. The scanning was developed with a step time of 2 s within 2θ range of 15-90° with a displacement of 0.02°. Further analysis was performed by field emission scanning electron microscopy (FE-SEM), JEOL model JSM-7600F, using a sharp LaB6 filament. A voltage of 5 kV and current intensity 70 μA were used to obtain the best image quality, to minimize charge accumulation and to avoid to damage the sample.

3. Results and discussion

3.1. Characterization

Figure 3 shows secondary electron (SE)-SEM image of the microstructure of the Ti6Al4V alloy in raw conditions from plate [Fig. 3a)] and filler ErTi5 wire [Fig. 3b)], both conditions showed regions with partially lengthened crystals with orientation towards the manufacture direction. Figure 3c) shows the morphology from deposits by CMT-WAAM that reveals some grains consisting of different α metastable phases as little colonies and acicular structures. Furthermore, CMT-WAAM deposits showed different zones thermally affected due to heat interaction between plate and filler wire during the deposition process. During material deposition and solidification, surge in temperatures promote the growth of smaller grains across grain boundaries where the internal energy is higher. Figure 3d) shows two different zones of

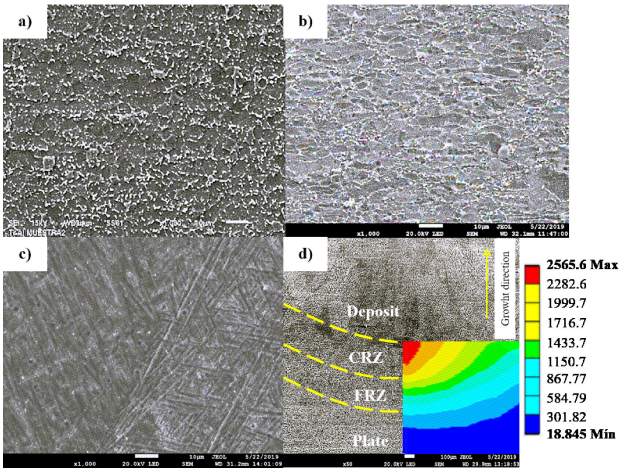

FIGURE 3. Microstructure characterization of Ti6Al4V alloy by SEM with secondary electrons; a) plate, b) filler ErTi5 wire, c) CMT-WAAM deposits and d) heat affected zones [22].

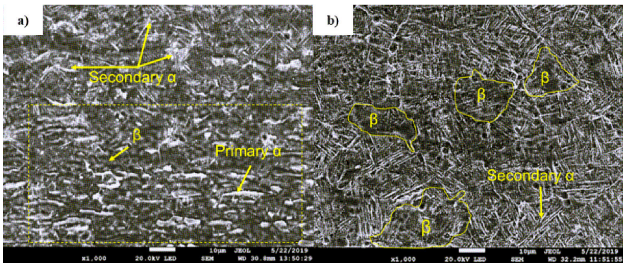

FIGURE 4. Secondary electron (SE)-SEM images of the microstructures of two different heat affected regions; a) fine recrystallization zone with laminated plate constituent and b) coarse recrystallization zone [22].

recrystallization which are caused by temperature gradients as shown by a thermal mapping. The thermal mapping was obtained by simulation modeling, using Ansys Mechanical APDL, and corresponds to the right half of the of the SEM image. With the help of the thermal mapping, it can be observed, a fine recrystallization zone (FRZ) and a coarse recrystallization zone (CRZ) with approximate thickness of 166 μm and 245 μm, respectively.

Figure 4 shows the microstructure of the different heat affected zones described in Fig. 3. The region that exhibited FRZ [Fig. 4a)] maintained the constituent morphology observed in the plate as received condition. The width of the laminar formations of $\alpha + \beta$ increased slightly as well as the α-grain size of original formation (primaries) which are lighter. In another work, Zeng *et al.* [23] mentioned that the low degree of transformation $\alpha \rightarrow \beta$ during cooling in that region is due to the influence of α secondary grains, which even, at reduced concentration is sufficient to prevent nucleation and growth of β grains.

The CRZ consists of a region that reached a maximum temperature, during processing, greater than or equal to the β transus temperature but lower than the melting temperature of Ti6Al4V deposit ($\beta_{\text{transus}} \leq T^{\circ} < T^{\circ}_{\text{Liquid}}$). An increase in temperature favors the grain growth and promotes the forma-

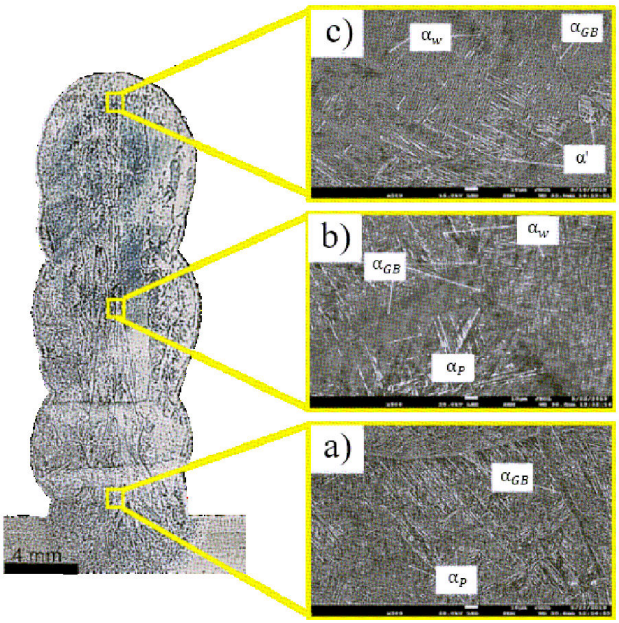

FIGURE 5. Optical microscope image (left) and secondary electron (SE)-SEM images (right) of the microstructures of Ti6Al4V deposit produced during CMT-WAAM [22].

tion of interfaces within the microstructure that lead to the growth of columnar regions [Fig. 4b)]. It is well known that overheating generates a decrease in the concentration of primary α grains, although the size of α grain increases. It is possible to observe the formation of primary β grains before completing the full transformation of $\alpha + \beta \rightarrow \beta$. It is also observed that the size of the grain increases near the melting zone.

Figure 5 shows the micro structure of Ti6Al4V deposit produced by CMT-WAAM. The different layers in the deposit were characterized in the transversal section. Each layer was 6 mm of length and 20% dilution percent with respect to subsequent layers. The constituent presented epitaxial growth, which was acquired during the multipass process. Higher magnification micrographs (Fig. 5) shows the different types of α constituents which are also reported elsewhere [24]. The first alpha-phase grains are formed at the grain boundaries of the still β-enriched crystals (αG_B). This first portion of α is eventually located in β grain boundaries that are either continuous or discontinuous. Figure 5a) shows the thin wall edge morphologies of α phase located at grain boundaries where ordered formations with similar orientation, called colonies, were also identified during the solidification when the β phase transform to α primary (α_p). In the central regions of the deposited wall basket-Widmanstätten structures (α_w) were found. This morphology is generated due to solidification of the last portion of the α-phase and is

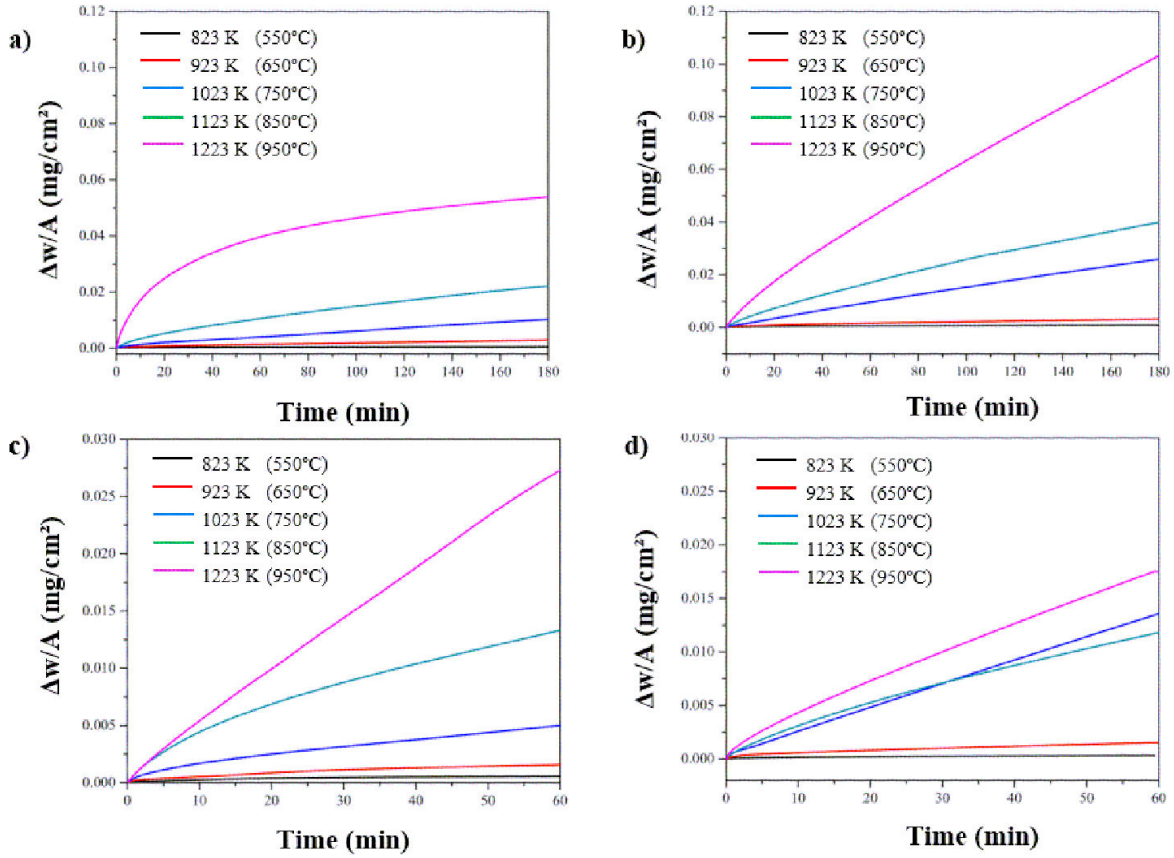

FIGURE 6. Isothermal oxidation of Ti6Al4V at different temperatures and the following conditions. a) CMT-WAAM deposits for 60 min, b) plate for 60 min, c) CMT-WAAM deposits for 180 min, and d) plate for 180 min.

retained within the still stable grains of the β-phase. Higher cooling rates promote the nucleation of this α_w phase from the remaining β-structures. A micrograph of this α_w phase along with clearly defined α-colonies are shown in Fig. 5b). Finally, large proportions of martensite constituent were identified in the prepared samples from the deposited walls. This metastable structure is identified as α', which was present in most of the deposit, and has also been reported by Corinne *et al*. [25] during WAAM processing under cooling conditions from 20 and up to 410 °C/s.

3.2. Oxidation behavior

Figure 6 shows weight gain of the Ti6Al4V samples from plate and deposits by WAAM-CMT after being exposed to Ar atmosphere at 823, 923, 1023, 1123 and 1223 K (550, 650, 750, 850 and 950°C) with two different oxidation times, namely, 60 and 180 min. Each weight measurement was divided by its specific surface area to obtain normalized data.

The results from the 60 min oxidation times are shown in Fig. 6a) for the deposits by CMT-WAAM and in Fig. 6b) for the plate. The additively manufactured specimen exhibited a linear weight gain until reaching the temperature of 1023 K (750°C). After 1023 K, the behavior of the weight gain curve begins to show a parabolic trend. This behavior can be described as a decrease in the rate of oxygen absorption as time increases. Regardless of the fabrication mode of Ti6Al4V, the oxidation kinetics showed and transient behavior from linear to parabolic mode at about 1023 K (750°C). These results are in agreement with that described by Pinilla *et al*. [26], who have defined an exponential behavior from 1023K (750°C) and a slower oxidation rate below this temperature.

Similarly, the thin-walled samples exposed for 180 min [Fig. 6c)] showed similar oxidation behavior below 1023 K (750°C) while the maximum oxidation rate occurs at 1223K (950 °C). In contrast, the plate sample [Fig. 6d)] shows a less parabolic as a function of time. Rajabi *et al*. [27] explained that the thermal oxidation for particles can be fitted to data whose governing reaction can be either limited by the product layer on the particle surface or limited by the rate of chemical reaction at the interface. They highlight the sub-linear behavior in the early stages of oxidation gradually changing to sub-parabolic behavior due to the reduction of the surface area available for the reaction. A diffusion phenomenon through the product layer on the surface of the thin-walled samples may explain the behavior of the oxidation kinetics at 1223 K (950°C), which was slower in contrast to the plate sample.

In the near-surface regions of Ti6Al4V samples, the tendency of the formation of an oxygen-enriched α-case has been studied [15,28-30]. The higher density of α-case limits further oxygen absorption. The surface energy can be higher in case of the deposits by CMT-WAAM generating higher oxidation kinetics in early stages of oxidation. As the α-case layer becomes thicker, the reaction kinetics decreases promoting the parabolic order law as shown in Fig. 6c). In this sense, the surface energy available on the sample plate should be less as the oxidation reaction maintains a constant growth with increasing time. This assumption can be validated with the development of a mathematical approach for the calculation of oxidation rate of Ti6Al4V for both conditions; deposits by CMT-WAAM and plate samples. The temperature dependence of the oxidation reaction as well as the activation energy, for both manufacturing processes of Ti6Al4V, was calculated using a linear fit of the Arrhenius equation:

$$K_p = Ae^{-\frac{E_a}{RT}}, \tag{1}$$

where K_p is the oxidation constant, A is the frecuency factor, E_a is the activation energy, R is the ideal gas constant (8.4143 J/ mol·K), and T is temperature. Equation (1) can be rewritten by taking the natural logarithm on both sides of the equation leading to Eq. (2). By plotting the inverse of temperature $(1/T)$ vs. $\ln(E_a)$, as shown in Fig. 7, the slope of the linear fit is the value of the activation energy (E_a) divided by the ideal gas constant.

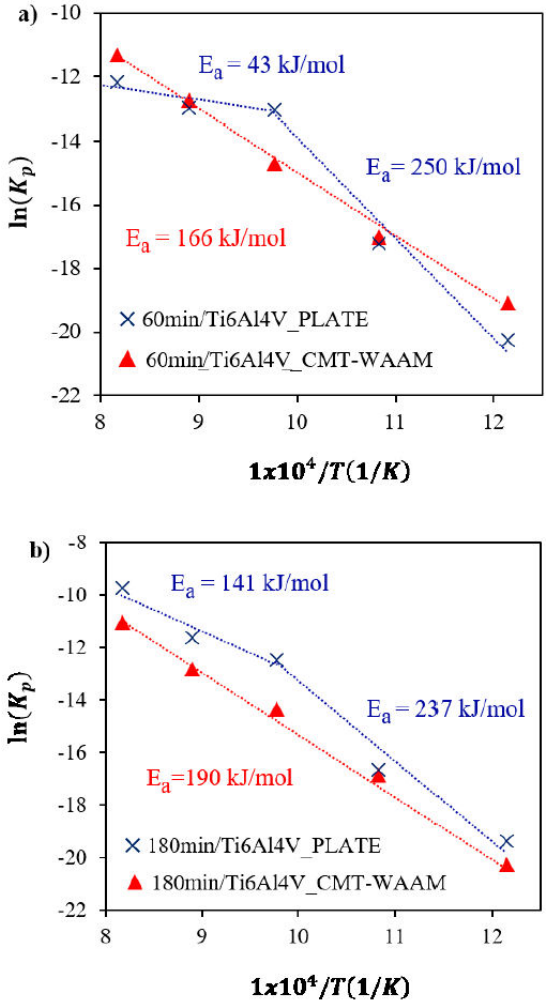

FIGURE 7. Activation energy for the oxidation of Ti6Al4V alloy at temperatures between 823 and 1223 K (550-950°C). a) 60 min of oxidation time b) 180 min of oxidation time.

$$\ln(K_p) = \ln(A) - \frac{E_a}{R}\left(\frac{1}{T}\right), \qquad (2)$$

where $y = \ln(K_p)$, $b = \ln(A)$, $m = E_a/R$, and $x = 1/T$.

The oxidation kinetics of the thin-walled samples showed a good linear fitting from 823 to 1223 K ($550 - 950$ °C) (see Fig. 7). On the contrary, the oxidized samples, obtained from the plate, exhibited an inflection point in the slope as shown in Fig. 7a) and 7b). The inflection in the slope coincides with the observed behavior in Fig. 6. The change in the slope can be defined as a change in the activation energy required for the oxidation reaction of Ti6Al4V.

The E_a values of the oxidation reaction (for the conditions analyzed in this work) were calculated from the slopes of the Arrhenius plots. The samples manufactured by CMT-WAAM treated for 60 and 180 min presented values of E_a of 166 kJ/mol and 190 kJ/mol, respectively. The difference in the E_a is about 12%, this can be attributed to the mayor resistance of the oxygen diffusion through the product layer for samples oxidized during 180 min. Similarly, the E_a values calculated for the Ti6Al4V plate samples are presented in Table III for oxidation times of 60 and 180 min. The kinetic behavior of plate samples were found to be different from that observed with the thin-walled sections due to a change in the slope of the curves for both isothermal oxidation times. For commercial plate in the temperature range of 823 to 1223 K ($550 - 750$ °C), the E_a was found to be 250 and 237 kJ/mol for isothermal oxidation times of 60 and 180 min, while for the analysis temperature range of 823 to 1223 K ($550 - 750$ °C), the E_a exhibited values of 43 and 144 kJ/mol for isothermal oxidation times of 60 and 180 min, respectively.

Higher values of E_a at temperatures below 1023 K (750 °C) can be related to the insufficient temperature to overcome the energy barrier; these values are close to each other (250 vs 237 kJ/mol). Also, below that processing temperature, a higher amount of energy is necessary than the required for the oxidation of the additively manufactured samples.

TABLE III. Parameters calculated to kinetics of oxidation Ti6Al6V alloy in both conditions; deposits by CMT-WAAM and plate.

Temperature		CMT-WAAM deposits		Plate	
°C	K	$(\Delta w/A)^2$	$\ln(Kp)$	$(\Delta w/A)^2$	$\ln(Kp)$
60 minutes					
550	823	3.09E-07	-19.08	9.44E-08	-20.26
650	923	2.49E-06	-17.00	2.01E-06	-17.21
750	1023	2.52E-05	-14.68	8.78E-05	-13.04
850	1123	1.78E-04	-12.73	1.39E-04	-12.97
950	1223	7.46E-04	-11.29	3.06E-04	-12.18
180 minutes					
550	823	2.89E-07	-20.25	6.96E-07	-19.371
650	923	8.59E-06	-16.85	1.06E-05	-16.648
750	1023	1.07E-04	-14.33	6.72E-04	-12.498
850	1123	4.93E-04	-12.80	1.59E-03	-11.637
950	1223	2.91E-03	-11.03	1.065E-02	-9.736

TABLE IV. Activation Energy reported by different authors in the literature.

Author	Temperature interval	E_a
Frangini [33]	873 - 973 K (600 - 700 °C)	147 kJ/mol
Guleryuz [30]	873 - 1073 K (600 - 800 °C)	233 kJ/mol
Anioek [29]	873 - 1073 K (600 - 800 °C)	274 kJ/mol
Yu Wei [17]	1123 - 1373 K (850 - 910 °C)	240 kJ/mol
Casadebaig [18]	773 - 873 K (500 - 600 °C)	250 kJ/mol
Casadebaig [19]	773 - 873 K (500 - 600 °C)	219 kJ/mol
Wei Guo [34]	673 - 1073 K (400 - 800 °C)	90 kJ/mol
CMT-WAAM (60 min)	823 - 1223 K (550 - 950 °C)	166 kJ/mol
CMT-WAAM (180 min)	823 - 1223 K (550 - 950 °C)	190 kJ/mol
Plate (60 min)	823 - 1023 K (550 - 750 °C)	250 kJ/mol
Plate (60 min)	1023 - 1223 K (750 - 950 °C)	43 kJ/mol
Plate (180 min)	823 - 1023 K (550 - 750 °C)	237 kJ/mol
Plate (180 min)	1023 - 1223 K (750 - 950°C)	141 kJ/mol

Table IV shows a summary of E_a values for the oxidation of Ti6Al4V from different authors [17,28,31,32], the E_a values calculated in this work are also included for plate and deposits manufactured by CMT-WAAM. It can be seen that the results calculated for plate for the temperature interval from 823 to 1223 K ($550 - 750$ °C) for both the oxidation times are consistent with other publications for a similar temperature range for Ti6Al4V manufactured by conventional casting and forging. However, the results of this work contrast with that presented by Yu Wei *et al*. [17] for the temperature range above 1023 K (750 °C); they obtained an E_a for the oxidation of Ti6Al4V as 240 kJ/mol for oxidation times of 180 min in circulating air atmosphere. As aforementioned, in this work, the E_a for commercial plate have been calculated as of 43 kJ/mol for an oxidation time of 60 min, and 141 kJ/mol at an oxidation time of 180 min in Ar atmosphere with a partial pressure of oxygen equals to 1×10^{-5} atm.

Moreover, the calculated E_a values for the additively manufactured samples are lower than the average values reported in the literature. Although Frangini *et al*. [33] obtained E_a a values close to those presented here, the samples were fabricated by conventional manufacturing and oxidized in air atmosphere; moreover, their oxidation measurements were performed without a high resolution equipment.

Figure 8 shows the oxidized surface of Ti6Al4V manufactured by CMT-WAAM confirming different degree of oxygen absorption due to processing conditions employed as the oxidation time increases. The oxide surface was characterized by X-ray diffraction (XRD). The sample oxidized for

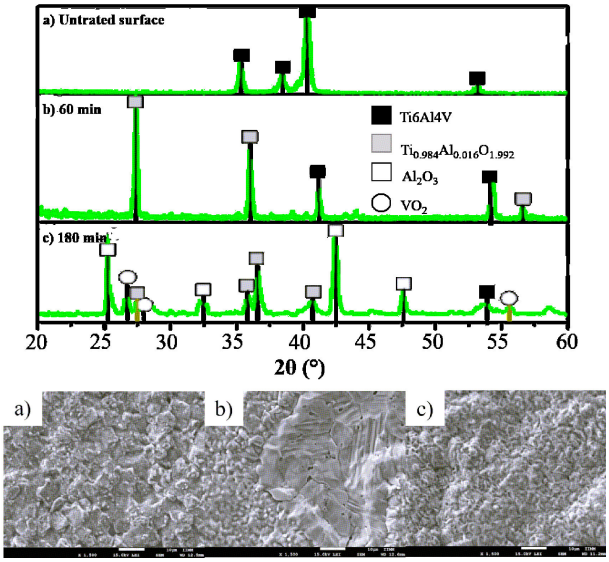

FIGURE 8. XRD analyses of the oxide layer of Ti6Al4V alloy from CMT-WAAM deposits.

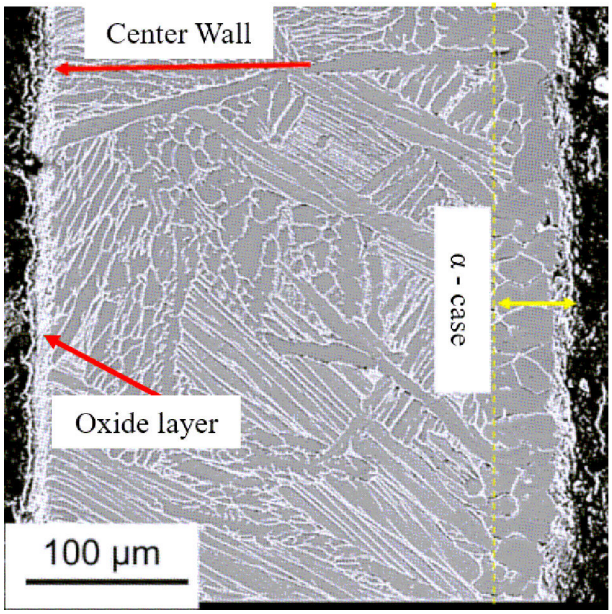

FIGURE 9. Secondary electron-SEM image showing oxygen diffusion zones resulting from the isothermal treatment at 950°C for 60 min for the CMT-WAAM deposits [22].

60 min reveals the presence of $Ti_{0.984}Al_{0.016}O_{1.992}$ (PDF 04-008-2608) and Ti6Al4V (PDF 00-044-1294) phases. The diffraction pattern for Ti6Al4V indicates that the product layer of oxidation must be very thin which is expected due to the low partial pressure of oxygen employed. On the other hand, the 180 min sample revealed the lowest amount of $Ti_{0.984}Al_{0.016}O_{1.992}$ due to the reaction of other alloy elements as Al is expected to form Al_2O_3 (PDF 04-013-6697) and V to produce VO_2 (PDF 04-012-6974). The elements as Al and V have a higher energy barrier to be overcome to initiate the oxidation reaction in contact with oxygen.

Figure 9 shows the stages of oxygen zone diffusion resulting from the isothermal treatment at 1223 K (950°C) for 60 min. On the right edge of the deposit by CMT-WAAM, it is possible to observe the formation of the α-case during the additive manufacturing; it reached an average thickness of 62 μm and extends along the sample along the edge of the deposit. On the opposite side of the sample, it was not possible to appreciate the α-case. Then, according to the micrograph, the oxidation process should be longer than 60 min to promote α-case formation. The oxide layer was revealed on both sides of the sample; however, the thickness of the oxide layer is not homogeneous. The effect of the formation of the oxide layer seems to be limited by the diffusion of the surface section of the sample where the sample section exhibited the presence of the α-case promoting the formation of about 12 μm oxide layer, while the other side showed the presence of about 32 μm oxide layer. The sensitivity of the oxidation reaction is limited by the diffusion of oxygen through the layer due to the saturation of oxygen in the α-case phase.

The obtained weight gain results demonstrate the reactivity of Ti6Al4V additively manufactured by CMT-WAAM as a function of isothermal processing time at temperatures between 823 and 1223 K (550 and 950°C) in Ar atmosphere. It was found that the amount of oxygen adsorption increases upon reaching the temperature of 1023 K (750°C) and increases as the temperatures increase. In other work, Wei *et al.* described a rapid increment in the degree of oxidation when $\alpha + \beta \rightarrow \beta$ in Ti6Al4V. They employed Eq. (3) to describe the oxidation kinetics as:

$$\left(\frac{\Delta w}{A}\right) = k_p t^{\frac{1}{n}}, \tag{3}$$

$$\theta = te^{-\frac{Q}{RT}}, \tag{4}$$

where Δw is the measured weight gain, A is the surface area of each sample, k_p is the oxidation rate constant, t is the oxidation time, and n is a rate exponent. The value of factor n is assumed to be 2 as considered for parabolic behavior [35]. They proposed a compensated temperature-time parameter as a normalized time unit and it is described and written in Eq. (3). The experimental points plotted on the graph $ln(\Delta w/A)$ versus $\ln(\theta)$ fit to a straight line

$$\ln\left(\frac{\Delta w}{A}\right) = 0.45\ln(\theta) + 2.53. \tag{5}$$

However, the results of the weight gain in this work have demonstrated that there is a phase transformation close to that temperature. Thus, the material microstructure plays an important role on the oxidation kinetics of Ti6Al4V. According to the experimental weight gain measurements, a linear fit was performed for data between 823 and 1023 K (550 and 750°C) using Eq. (6), while for temperatures from 1023 K (750°C) up to 1223 K (950°C) Eq. (7) was used as shown in Fig. 10.

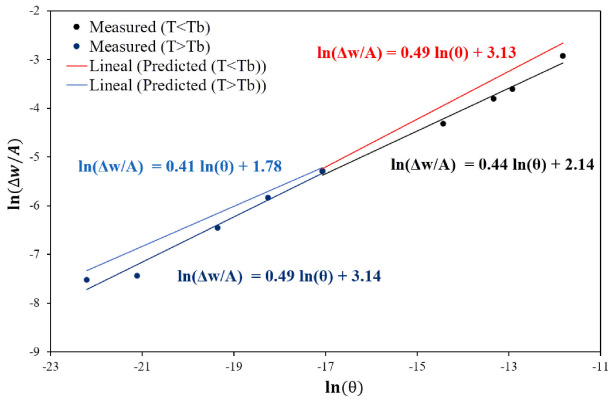

FIGURE 10. Arrhenius plot of the experimental data for the calculation of the activation energy of Ti6Al4V manufactured by CMT-WAAM in the range of 823 to 1223 K.

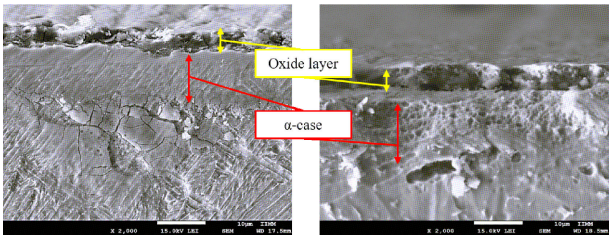

FIGURE 11. SEM image of the Ti6Al4V samples fabricated by CMT-WAAM treated for: a) 60 min and b) 180 min.

$$\ln\left(\frac{\Delta w}{A}\right) = 0.49\ln(\theta) + 3.13, \tag{6}$$

$$\ln\left(\frac{\Delta w}{A}\right) = 0.41\ln(\theta) + 1.78. \tag{7}$$

Experimental data in Fig. 11 shows a micrograph of the Ti6Al4V thin-walled samples treated for 60 min [Fig. 11a)] and 180 min [Fig. 11b)], which reveals the growth of an oxide layer between 5 and 8 μm in the shallowest section of the sample. In addition,the formation of the α-case layer in early stages of reaction, during 60 min treatment with a cracking section, is gradually grown due to the oxygen saturation in regions with volumetric defects since sample manufacture. At 180 min of treatment, the largest size in surface oxide layer was obtained, as well as a saturation phenomenon in the α-case region with rough surface appearance, but higher density and extent. The oxygen saturation in the reaction product layer as well as the saturation of the α-case prove not to limit the progress of the oxidation reaction once the required activation energy has been overcome as a function of temperature.

4. Conclusions

In this work, the isotermal oxidation behavior of Ti6Al4V alloy at 823-1223K (550-950°C) for 60-180 min in Ar atmosphere with an oxygen partial pressure of 1×10^{-5} atm, as impurity, was investigated. For both oxidation times the rate of the oxidation reaction is faster in the early stages of reaction. Furthermore, the oxidation rate increases after 1023 K (750°C) for both conditions. The oxidation constant (k_p) was higher for the CMT-WAAM deposits for an oxidation time of 60 min, while for 180 min the k_p constant is higher for the plate samples. The activation energy (E_a) for oxide formation in the CMT-WAAM deposits decreased by 33% for 60 min and 19% for 180 min compared to the plate samples, for which, a slope change occurred at 1023 K (750°C) for both oxidation times. The α-case region for the CMT-WAAM deposits was found at conditions of 60 min-823 K (550°C), 60 min-1023 K (750°C), 60 min-1223 K (950°C), and 180 min-823 K (550°C). The correlation coefficient of the mathematical model for $T°> T_\beta$ is 96%, while for $T°< T_\beta$, the correlation coefficient is 98%.

Acknowledgment

Authors are thankful to CONAHCYT for grants given to J.E. Ordaz-Cervantes and E. Reyes-Gordillo.

Competing interests

The authors declare that they have no known competing financial interests or personal relationships that could have appeared to influence the work reported in this paper.

1. S. W. Williams *et al.*, Wire + Arc additive manufacturing, *Materials Science and Technology* (United Kingdom) **32** (2016) 641, https://doi.org/10.1179/1743284715Y.0000000073.

2. Y. Li, C. Su, and J. Zhu, Comprehensive review of wire arc additive manufacturing: Hardware system, physical process, monitoring, property characterization, application and future prospects, *Results in Engineering* **13** (2022) 100330, https://doi.org/10.1016/j.rineng.2021.100330.

3. T. DebRoy *et al.*, Additive manufacturing of metallic components - Process, structure and properties, *Progress in Materials Science* **92** (2018) 112, https://doi.org/10.1016/j.pmatsci.2017.10.001.

4. T. Artaza *et al.*, Wire arc additive manufacturing Ti6Al4V aeronautical parts using plasma arc welding: Analysis of heattreatment processes in different atmospheres, *Journal of Materials Research and Technology* **9** (2020) 15454, https://doi.org/10.1016/j.jmrt.2020.11.012.

5. X. Wang *et al.*, Process stability for GTAW-based additive manufacturing, *Rapid Prototyping Journal* **25** (2019) 809, https://doi.org/10.1108/RPJ-02-2018-0046.

6. S. Pattanayak and S. K. Sahoo, Gas metal arc welding based

additive manufacturing-a review, *CIRP Journal of Manufacturing Science and Technology* **33** (2021) 398, https://doi.org/10.1016/j.cirpj.2021.04.010.

7. A. Schierl, The CMT - Process - A Revolution in welding technology, Welding in the World **49** (2005) 38.
8. F. yuan SHU *et al.,* FEM modeling of softened base metal in narrow-gap joint by CMT+P MIX welding procedure, *Transactions of Nonferrous Metals Society of China* **24** (2014) 1830, https://doi.org/10.1016/S1003-6326(14)63260-X.
9. F. Martina *et al.,* Tandem metal inert gas process for high productivity wire arc additive manufacturing in stainless steel, *Additive Manufacturing* **25** (2019) 545, https://doi.org/10.1016/j.addma.2018.11.022.
10. Z. Lin, K. Song, and X. Yu, A review on wire and arc additive manufacturing of titanium alloy, *Journal of Manufacturing Processes* **70** (2021) 24, https://doi.org/10.1016/j.jmapro.2021.08.018.
11. J. Gou *et al.,* Effect of cold metal transfer mode on the microstructure and machinability of Ti-6Al-4V alloy fabricated by wire and arc additive manufacturing in ultra-precision machining, *Journal of Materials Research and Technology* **21** (2022) 1581, https://doi.org/10.1016/j.jmrt.2022.10.011.
12. S. Panicker *et al.,* Investigation of thermal influence on weld microstructure and mechanical properties in wire and arc additive manufacturing of steels, *Materials Science and Engineering: A* **853** (2022) 143690, https://doi.org/10.1016/j.msea.2022.143690.
13. S. Thapliyal, Challenges associated with the wire arc additive manufacturing (WAAM) of aluminum alloys, *Materials Research Express* **6** (2019) 112006, https://doi.org/10.1088/2053-1591/ab4dd4.
14. A. Caballero *et al.,* Oxidation of Ti-6Al-4V during Wire and Arc Additive Manufacture, *3D Printing and Additive Manufacturing* **6** (2019) 91, https://doi.org/10.1089/3dp.2017.0144.
15. H. Guleryuz and H. Cimenoglu, Oxidation of Ti-6Al-4V alloy, *Journal of Alloys and Compounds* **472** (2009) 241, https://doi.org/10.1016/j.jallcom.2008.04.024.
16. R. Gaddam *et al.,* Oxidation and alpha-case formation in Ti-6Al-2Sn-4Zr-2Mo alloy, *Materials Characterization* **99** (2015) 166, https://doi.org/10.1016/j.matchar.2014.11.023.
17. Dong E. *et al.,* High-Temperature Oxidation Kinetics and Behavior of Ti-6Al-4V Alloy, *Oxidation of Metals* **88** (2017) 719, https://doi.org/10.1007/s11085-017-9770-0.
18. A. Casadebaigt, J. Hugues, and D. Monceau, Influence of Microstructure and Surface Roughness on Oxidation Kinetics at 500-600°C of Ti-6Al-4V Alloy Fabricated by Additive Manufacturing, *Oxidation of Metals* **90** (2018) 633, https://doi.org/10.1007/s11085-018-9859-0.
19. A. Casadebaigt, J. Hugues, and D. Monceau, High temperature oxidation and embrittlement at 500-600 °Cof Ti-6Al-4V alloy fabricated by Laser and Electron Beam Melting, *Corrosion Science* **175** (2020) 108875, https://doi.org/10.1016/j.corsci.2020.108875.
20. A. S. Khanna, Chapter 6 - High-Temperature Oxidation, In M. Kutz, ed., Handbook of Environmental Degradation of Materials (Third Edition), third edition ed., pp. 117-132 (William Andrew Publishing, 2018), https://doi.org/10.1016/B978-0-323-52472-8.00006-X,
21. ISO/ASTM, Additive Manufacturing - General Principles Terminology (ASTM52900), *Rapid Manufacturing Association* (2013) 10, https://doi.org/10.1520/F2792-12A.
22. E. Reyes-Gordillo *et al.,* Determination and effect of cold metal transfer parameters on Ti6Al4V multi-layer deposit during wire arc additive manufacturing, *Welding in the World* **67** (2023) 1629, https://doi.org/10.1007/s40194-023-01511-9.
23. L. Zeng and T. Bieler, Effects of working, heat treatment, and aging on microstructural evolution and crystallographic texture of, and phases in Ti-6Al-4V wire, *Materials Science and Engineering: A* **392** (2005) 403, https://doi.org/10.1016/j.msea.2004.09.072.
24. L. Wanying *et al.,* Effect of Different Heat Treatments on Microstructure and Mechanical Properties of Ti6Al4V Titanium Alloy, *Rare Metal Materials and Engineering* **46** (2017) 634, https://doi.org/10.1016/S1875-5372(17)30109-1.
25. C. Charles Murgau, Microstructure model for Ti-6Al-4V used in simulation of additive manufacturing (Doctoral dissertation, Lulea tekniska universitet, 2016). https://api.semanticscholar.org/CorpusID:139365537.
26. M. Bautista *et al.,* Microstructural characterization of titanium alloy Ti6Al4V thermally oxidized/Caracterización microestructural de la aleación de titanio Ti6Al4V oxidada térmicamente, *Prospectiva* **16** (2018) 68, https://doi.org/10.15665/rp.v16i2.1617.
27. A. Rajabi, A. Mashreghi, and S. Hasani, Non-isothermal kinetic analysis of high temperature oxidation of Ti-6Al-4V alloy, *Journal of Alloys and Compounds* **815** (2020) 151948, https://doi.org/10.1016/j.jallcom.2019.151948.
28. K. Aniolek *et al.,* Mechanical and tribological properties of oxide layers obtained on titanium in the thermal oxidation process, *Applied Surface Science* **357** (2015) 1419, https://doi.org/10.1016/j.apsusc.2015.09.245.
29. K. Aniolek, M. Kupka, and A. Barylski, Sliding wear resistance of oxide layers formed on a titanium surface during thermal oxidation, *Wear* **356** (2016) 23, https://doi.org/10.1016/j.wear.2016.03.007.
30. H. Guleryuz and H. Cimenoglu, Surface modification of a Ti-6Al-4V alloy by thermal oxidation, *Surface and Coatings Technology* **192** (2005) 164, https://doi.org/10.1016/j.surfcoat.2004.05.018.
31. D. Brice *et al.,* Oxidation behavior and microstructural decomposition of Ti-6Al-4V and Ti-6Al-4V-1B sheet, *Corrosion Science* **112** (2016) 338, https://doi.org/10.1016/j.corsci.2016.07.032.
32. A. Casadebaigt, J. Hugues, and D. Monceau, Influence of Microstructure and Surface Roughness on Oxidation Kinetics at 500-600°C of Ti-6Al-4V Alloy Fabricated by Additive Manufacturing, *Oxidation of Metals* **90** (2018) 633, https://doi.org/10.1007/s11085-018-9859-0.

33. S. Frangini, A. Mignone, and F. de Riccardis, Various aspects of the air oxidation behaviour of a Ti6Al4V alloy at temperatures in the range 600-700 °C, *Journal of Materials Science* **29** (1994) 714, https://doi.org/10.1007/BF00445984.

34. W. Guo *et al.*, Effect of laser shock processing on oxidation resistance of laser additive manufactured Ti6Al4V titanium alloy, *Corrosion Science* **170** (2020) 108655, https://doi.org/10.1016/j.corsci.2020.108655.

35. J. M. Alvarado-Orozco *et al.*, First stages of oxidation of Pt-modified nickel aluminide bond coat systems at low oxygen partial pressure, *Oxidation of Metals* **78** (2012) 269, https://doi.org/10.1007/s11085-012-9305-7.